IEEE Access
Multidisciplinary | Rapid Review | Open Access Journal

Received July 6, 2020, accepted July 14, 2020, date of publication July 22, 2020, date of current version July 31, 2020.

Digital Object Identifier 10.1109/ACCESS.2020.3011136

Assessment of the Inner Surface Roughness of 3D Printed Dental Crowns via Optical Coherence Tomography Using a Roughness Quantification Algorithm

JAEYUL LEE[1], SM ABU SALEAH[1], BYEONGGYU JEON[1], RUCHIRE ERANGA WIJESINGHE[2,3], DONG-EUN LEE[4], MANSIK JEON[1], (Member, IEEE), AND JEEHYUN KIM[1], (Member, IEEE)

[1]School of Electronics Engineering, College of IT Engineering, Kyungpook National University, Daegu 41566, South Korea
[2]Department of Biomedical Engineering, College of Engineering, Kyungil University, Gyeongsan 38428, South Korea
[3]Department of Autonomous Robot Engineering, College of Smart Engineering, Kyungil University, Gyeongsan 38428, South Korea
[4]School of Architecture, Civil, Environment, and Energy Engineering, Kyungpook National University, Daegu 41566, South Korea

Corresponding authors: Dong-Eun aLee (dolee@knu.ac.kr) and Mansik Jeon (msjeon@knu.ac.kr)

This study was supported by BK21 Plus project funded by the Ministry of Education, Korea (21A20131600011). This research was supported by the National Research Foundation of Korea (NRF) grant funded by the Korea government, MSIT (No. NRF-2018R1A5A1025137), the Ministry of Education (No. 2018R1D1A1B07043340), and MSIP (No. 2017M3A9E2065282).

ABSTRACT Dental crowns are used to restore decayed or chipped teeth, where their surfaces play a key role in this restoration process, as they affect the fitting and stable bonding of the prostheses. The surface texture of crowns can interfere with this restoration process, therefore the measurement of their inner surface roughness is very important but difficult to achieve using conventional imaging methods. In this study, the inner surfaces of dental crowns were three-dimensionally (3D) visualized using swept-source optical coherence tomography (SS-OCT) system. Nine crowns were fabricated with a commercial 3D printer using three different hatching methods (one-way, cross, and 30° angle counter-clockwise) and three different build direction angles (0°, 45°, and 90°). In addition, an image processing algorithm was developed, which uses morphological filtering, boundary detection, and a high-pass frequency filtering technique, to quantitatively evaluate the inner surface roughness of the dental crowns cross-sections with the depth-of-focus set to match two different regions. The averaged smoothness of fabricated crown was effectively produced using the cross-hatching and the build direction angle of 90° by the respective process. Thus, the results confirm the potential use of this methodology to determine the best parameters to use in 3D fabrication for improving the effectiveness and stability of dental prostheses.

INDEX TERMS 3D printing, dental crown, image processing, optical coherence tomography, surface roughness.

I. INTRODUCTION

Dental prostheses are widely used in clinical treatment to restore decayed or chipped teeth [1], [2]. A dental crown is a restorative prosthesis that involves the complete or partial covering of a tooth or dental implant. Prostheses such as these are generally prepared using casting [3], milling [4], [5], lost-wax (LW) [6], and three-dimensional (3D) printing [7], [8] methods. The casting method is time-consuming, and due to high tooling costs, a high production volume is required. Milling is a high-cost process with high material waste, unlike the 3D printing method, which produces better quality products, allows fast fabrication, has almost no restriction in terms of product shape, and is cost-effective. In 3D printing, the build direction has a direct impact on the dimensional accuracy of a 3D printed dental crown [9], and for different build directions, different root mean square estimate values have been observed [10]. Computer-aided design/computer-aided manufacturing (CAD/CAM), selective laser melting (SLM), rapid prototype, and direct inkjet printing are some examples of 3D printing technology.

The surface roughness of a dental prosthesis can have a direct or indirect impact on bacterial plaque retention, staining, oral health, and patient comfort, [11]–[14] thus, a well-polished smooth surface is the most significant

The associate editor coordinating the review of this manuscript and approving it for publication was Mehul S. Raval.

advantage of a 3D printed dental prosthesis. If the surface of a dental crown is not sufficiently polished, dental restoration can be difficult, resulting in the accumulation of plaque, gingival irritation, and poor aesthetics due to surface roughness [15]. Moreover, the surface roughness of dental crowns influences the discoloration, abrasion, and aesthetic appearance of the dental prostheses [16]. Thus, it is essential to be able to assess the roughness of their inner surface to develop superior dental crowns with enhanced restoration efficiency for dental crown treatment. The inner surface roughness of a 3D printed dental prosthesis plays an important role in its successful bonding with a tooth. Recently, several techniques have been developed for the assessment of surface roughness. Among them, an optical profilometer has been used to determine average surface roughness, where low average roughness values are considered to represent a smooth surface, while higher average roughness values are considered to represent a rough surface [17]. Scanning electron microscopy (SEM) imaging is one of the techniques most widely used to measure the surface roughness of enamel and dentine in teeth [18]. However, SEM has a few limitations when it comes to measuring the roughness of a sample surface. It is an expensive technique, the system as a whole is bulky, sectioning of the sample is required in most cases, and the microscope has to be housed in an electrical, magnetic, and vibration-free environment. The surface characteristics of resin composites have been assessed using a gloss meter, which measures the reflection gloss of a sample surface, where higher gloss values were measured from smoother resin materials [19]. Over the past two decades, atomic force microscopy (AFM) has been used in the dental equipment research field to capture 3D topographical images of surface roughness at nanometer resolution. However, the fixing of the sample in a fluid substrate limits the applicability of this method. Moreover, in AFM, the vertical motion of the tip is limited to 5–15 μm [20], and a slow scan time and single scan image size (150 $\times$ 150 μm) are also other notable limitations of this technique. Contact profilometry is a technique used for scanning the topography of a sample surface, but it is not well suited to very soft, liquid, and easily damaged surfaces. The stylus of a profilometer can also be damaged when used to scan a very hard surface. Conventional imaging methods have some limitations to assess the whole inner surface of the dental crown. Because ultrasound has low axial and lateral resolution and it requires the use of gel as a coupling agent [21]. Confocal laser scanning microscopy is limited by low penetration depth (400-500 μm) and a limited scan area (500 $\times$ 500 μm^2) [22]. X-ray, computed tomography, and magnetic resonance imaging (MRI) have a low spatial resolution range (0.5 – 1 mm) [23]–[25]. Therefore, an optical non-invasive imaging method is required to evaluate the surface roughness of materials.

Optical coherence tomography (OCT) is an optical imaging modality used to conduct high-resolution, cross-sectional imaging of inner microstructures in materials and biological structures by measuring the echo time delay and backscattered light magnitude [26], which can overcome the aforementioned limitations of other conventional imaging and roughness measurement techniques. OCT can be classified into Fourier-domain and time-domain. Fourier-domain OCT can be further classified into spectral-domain OCT (SD-OCT) and swept-source OCT (SS-OCT) [27]. SS-OCT has deeper penetration and faster image acquisition time compared with other OCT systems and the light source of this system is divided into a spectrum through a tunable laser instead of a super-luminescent diode [28]. OCT has been widely applied in medical diagnosis [29]–[34], entomological studies [35], [36], industrial applications [37]–[39], and in the agricultural field [40], [41]. Nowadays, with developments being made in terms of the size of systems and types of light sources, OCT could be used for the advanced diagnosis of tooth decay and periodontal disease [42]. A polarization-sensitive OCT system has previously been employed to assess dental structures and the obtained results were compared with those of other conventional OCT systems [43]. In our previously reported studies, we used OCT to quantitatively assess dental caries [44], to measure inner and marginal discrepancies in dental prostheses [45], to classify human gingival sulcus structure [46], to identify human gingival sulcus [47], to analyze enamel loss [48], and to characterize micro-damage in cortical bone [49].

In this study, dental crown samples were prepared by using a 3D printer, and then OCT imaging of the prepared samples was performed by using the SS-OCT imaging system. An image processing algorithm was developed for the numerical evaluation of dental crown inner surface roughness based on the acquired OCT images. The proposed OCT-based methodology can be used in dental restoration to measure surface roughness and simultaneously to determine the performance of different hatching methods and build directions of 3D printed samples after their fabrication, which will be useful both for industry and researchers in the field of the fabrication of materials for dental restoration.

II. MATERIALS AND METHODS

A. PREPARATION OF THE DENTAL CROWN SAMPLES

Figure 1(a) shows the SLM technique used in the fabrication of dental crowns. In SLM, high-temperature laser light is used to fabricate the samples, via either the sintering or welding of parts in a powder bed, where the object is printed by forming one layer on top of another, as the sample holding platform moves down and the powder delivery platform moves up accordingly [50]. A commercial 3D printer (ReaLizer SLM 125) equipped with a laser source with 200 W power, which can achieve high accuracy and high surface quality printing of tiny modules were used to fabricate dental crown samples, with an accuracy of 30–60 μm. The optical system of this 3D printer was digitally regulated using F-theta optics at 100° C under a flow of argon gas at ca. 35 L/h, with a construction volume (X $\times$ Y $\times$ Z) of 125 mm $\times$ 125 mm $\times$ 200 mm. The values of utilized parameters such as hatching distance, hatch offset, point distance and laser exposure time were

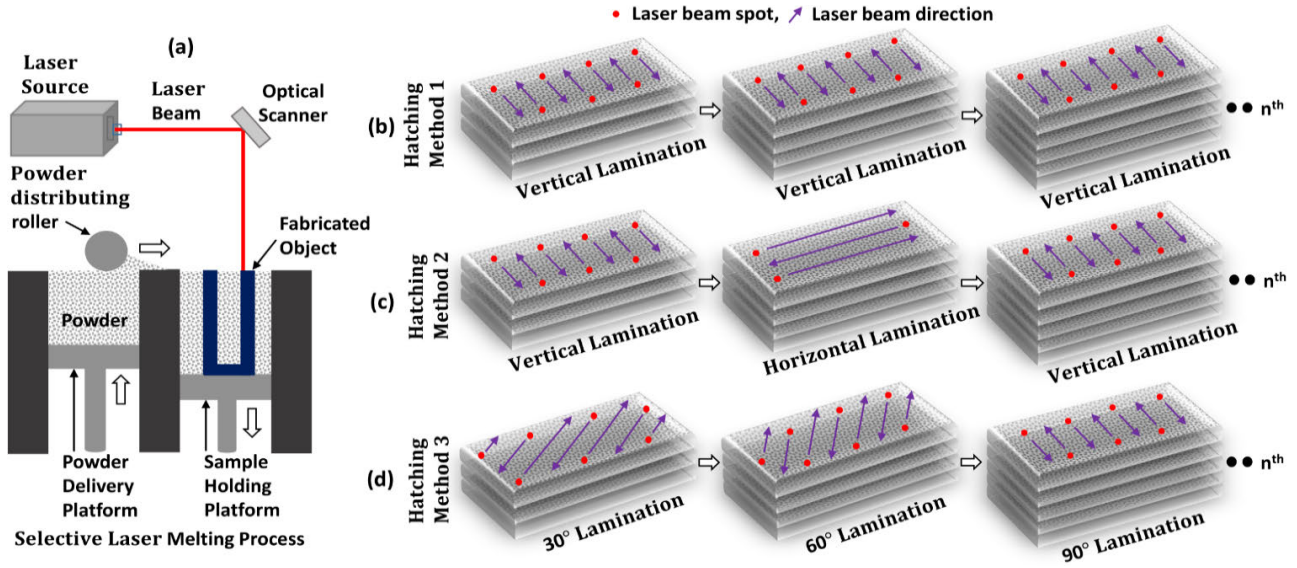

FIGURE 1. Selective laser melting (SLM) process and hatching methods of the 3D fabrication of dental crowns. (a) Schematic of the SLM process. (b) Hatching method 1, in which layer stacking is achieved by moving the laser pointer back and forth in one direction. (c) Hatching method 2, in which layer stacking is achieved by printing one layer on top of another in such a way that they are perpendicular to each other. (d) Hatching method 3, where layer stacking is achieved by turning the laser pointer 30° counter-clockwise after the printing of each layer.

0.08 mm, 0.04 mm, 20 μm, 60 μs, respectively. The parameters were fixed to keep the control condition during the 3D fabrication of the dental crowns using three hatching methods. The lamination thickness in 3D printing was fixed at 0.025 mm. So the calculated number of layers to fabricate a single dental crown sample of 11 mm height is 440 (11/0.025, sample height/lamination thickness). 440 layers were stacked on top of another to form a single dental crown sample of 11 mm height. Chrome–cobalt was used as a raw material, which was subjected to three different hatching methods with three different build directions to print different dental crown samples. In all three hatching methods, the laser energy, scan velocity, and laser lamination thickness were constantly maintained. The three different hatching methods used to fabricate dental crowns are shown in Figures 1(b–d). In this study, the build direction of the fabricated dental crown was with respect to the support structure of the dental crown. Hatching method 1 involves one-way vertical lamination, i.e., moving the laser pointer back and forth in one direction. After forming one layer, the stacking of the next layer of the sample was started from the same lamination angle after completing the previous layer. Figure 1(b) shows a schematic diagram of the one-way lamination of hatching method 1. In hatching method 2, shown in Figure 1(c), the hatching was carried out via a two-way vertical and horizontal alternating lamination (cross lamination at 0° and 90°) process. In this method, the first layer was vertically stacked followed by the horizontal stacking of the second layer (i.e., the stacked layers are perpendicular to each other), then the next successive layer was printed vertically once again, and this process was continued until all of the layers of the sample had been stacked on one another. In hatching method 3, shown in Figure 1(d), the layer stacking was carried out by turning the laser pointer counter-clockwise by an angle of 30°. The first layer was stacked at an angle of 30°, then the second layer was stacked at an angle of 60°, and following this, the third layer was stacked at an angle of 90° (all three angles are in respect to the initial position of the laser pointer). This 30° angle counter-clockwise lamination was continued until the sample fabrication was complete. Figure 2(a) shows 3D models of the dental crowns with the build directions and support structure. A photograph of the fabricated dental crown samples is shown in Figure 2(b). Since the main purpose of this study was to determine the most appropriate hatching method and build direction by assessing the inner surface roughness through roughness quantification algorithm, no post-processing was performed that affects the inner surface roughness of the dental crown After 3D fabrication. The use of post-processing methods like sandblasting, soot peening, grinding, electropolishing, etc. may increase the surface smoothness but it would affect the goal of this study of roughness assessment. Once the samples were completely fabricated, two-dimensional (2D) and 3D OCT imaging was carried out. 500 successive cross-sectional 2D images were obtained to make one 3D image. The volumetric samples were rendered and analyzed in all three section planes (sagittal, coronal, and orthogonal).

B. EXPERIMENTAL SETUP OF THE SS-OCT SYSTEM

A schematic diagram of the SS-OCT system (OCS1310V1, Thorlabs, Inc., Newton, New Jersey, USA) used for imaging of the dental crown samples is shown in Figure 3. This commercially available system comprises a swept-source laser engine with a central wavelength of 1310 nm and full width half maximum bandwidth of >97 nm (−10 dB cut-off point). The average laser output power from the source is >20 mW, and its axial scan rate is 100 kHz. The lateral and

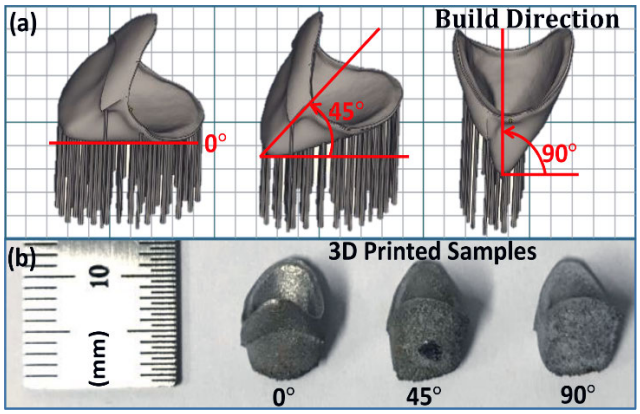

FIGURE 2. Build directions used in the fabrication process and printed dental crown samples. (a) Modeling of dental crowns with the build directions shown with respect to the support. (b) Photograph of the 3D printed dental crowns after removing their support structures.

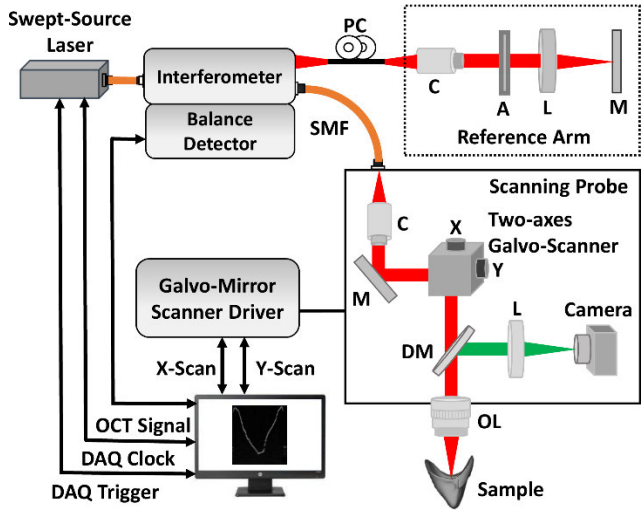

FIGURE 3. Schematic of the SS-OCT system. A: attenuator; C: collimator; DM: dichroic mirror; DAQ, data acquisition board; L: lens; M: mirror; OL: object lens; PC: polarization controller; SMF: single-mode fiber.

axial resolutions of the system are 25 μm and <16/12 μm (air/water), respectively. At zero optical-path length difference, the sensitivity is 111 dB. The maximum scanning range and imaging depth of the system are 10 and 12 mm, respectively, and the maximum imaging volume size (L × W × D) is 10 mm × 10 mm × 12 mm, with a maximum sampling resolution (L × W × D) of 1024 ×1024 × 2048 pixels. A detailed explanation of the system specifications can be found in the previous literature [35].

C. IMAGE PROCESSING ALGORITHM

The inner surface averaged roughness of the dental crown samples was measured by analyzing the acquired 2D OCT images. The cross-sectional OCT images with a complete (throughout) focused inner surface were required to calculate the entire inner surface roughness of the dental crown. Imaging of the entire inner surface of the dental crown in once with a complete focus was challenging, due to the height of the dental crown. Thus, the entire inner surfaces of the dental crowns were imaged twice with the depth-of-focus (DOF) set at two different regions of the dental crown to obtain fully focused inner surface OCT images of the samples. In the first attempt, the DOF was set at the bottom region of the dental crown, and in the second, the DOF was set at the topmost region of the dental crown, to produce two different groups of images for analysis and calculating the roughness of the samples. The 9 samples of the dental crown were fabricated by the combination of three hatching methods and three build directions using the commercial 3D-printer. After 3D fabrication, each sample was imaged by setting the depth of focus (DOF) at the top and bottom regions of the sample. For nine dental crown samples, a total of 18 (9 samples ×2 positions) volumes of OCT images were acquired by the SS-OCT system. The one-volume image consisted of 500 cross-sectional OCT images. The region of interest (ROI) of the focused top and bottom regions were analyzed by the customized image processing algorithm. Figure 4 illustrates the overall steps involved in the roughness calculating processes.

1) IMAGE PROCESSING FOR THE IMAGES WITH DOF SET AT BOTTOM REGION OF THE DENTAL CROWN

Figures 4(a–d) show some important image processing steps applied to the images with the DOF set at the bottom region of the dental crown. In the first step, cross-sectional OCT images were loaded into the MATLAB (R2016a) platform, and then RGB to grayscale conversion was carried out. Next, morphological filtering was applied to remove the small object or noise, especially the inner surface boundary adjacent noise as well as to preserve the same shape or information of the inner surface boundary. The morphological operation made the measurements look smoother by removing the noise and as the inner surface boundary shape or information was preserved, the final roughness values were not affected. In morphological filtering, a square structuring element with a three-pixel width was used to perform a morphological opening of the grayscale images, by processing them pixel by pixel according to their neighboring pixel values. The morphological opening is an erosion operation followed by a dilation operation, using the same structuring element for both operations. After the morphological filtering, the left and right sides of the images were excluded, the middle region of the image was selected as the ROI, and image binarization was carried out. In the image binarization process, grayscale images were converted into binary images by replacing all pixels in the input images with luminance higher than level (predefined threshold value, 50/255) with the value 1 (white) and replacing all other pixels with the value 0 (black). After the image binarization process, the inner surface boundary was detected by searching each column pixel of the image array from the top where the pixel values were "1" for the first time. In this search process, when "1" was detected, the corresponding row index value was taken as the part of the inner surface boundary and continued the searching to make a graph for the whole inner surface boundary of the crown. Then a high-pass frequency filtering operation was performed on the acquired dental crown inner surface

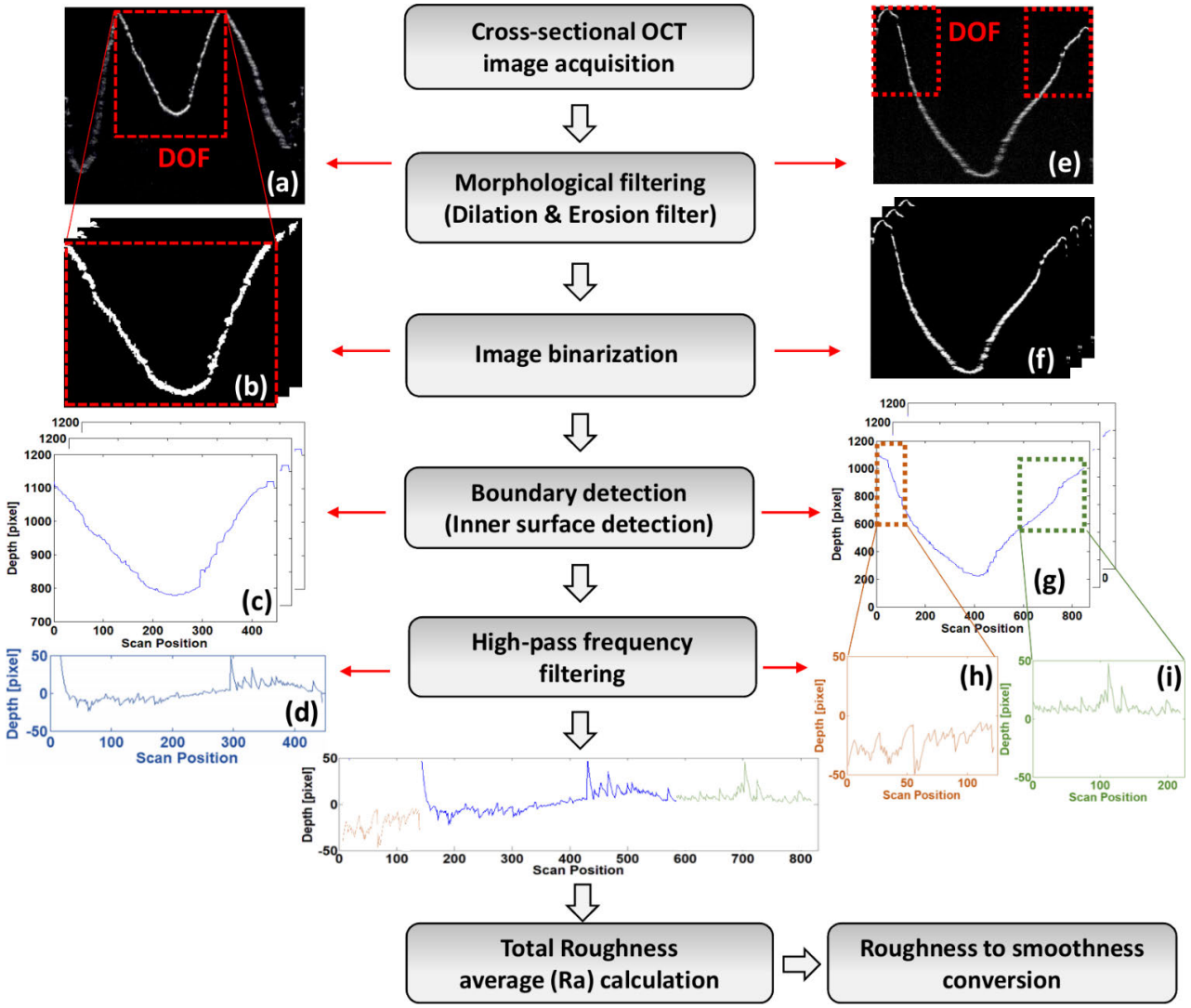

FIGURE 4. Image processing algorithm for the measurement of averaged roughness. Images (a, b, c, and d) belongs to the images with DOF at the bottom region of the dental crown. Images (e, f, g, h, and i) belongs to the images with DOF at the topmost region of the dental crown.

boundary signal. A typical 3D printed surface has three different frequency ranges, which can be classified as follows: low frequency or higher wavelength components are referred to as form, the medium frequencies as waviness, and higher frequencies or short-wavelength components as roughness. In high-pass frequency filtering, signals with a frequency higher than a pre-defined cut-off frequency are considered for further processing. A first-order Butterworth filter was used with filter parameters such as cut-off, sampling, and Nyquist frequencies of 2.8 Hz, 100 Hz, and 50 Hz, respectively for the evaluation of surface roughness in high-pass frequency filtering. After the high-pass frequency filtering, the averaged roughness was calculated from the average of the absolute value of the roughness profile.

2) IMAGE PROCESSING FOR THE IMAGES WITH DOF SET AT TOPMOST REGION OF THE DENTAL CROWN

Figures 4(e–i) show some important image processing steps applied to the images with the DOF set at the topmost region of the dental crown. After loading 2D OCT images into the MATLAB (R2016a) platform, RGB to grayscale conversion, morphological filtering, image binarization, and inner surface boundary detection was carried out according to the method described in the previous section. After detecting the inner surface boundary, the focused left and right sides were separated from the partially focused middle part of the dental crown. This was followed by high-pass frequency filtering, which was applied to the separated left and right sides of the inner surface boundary signal.

After high-pass frequency filtering, the averaged roughnesses of the left and right-side signals were calculated from the absolute values of their roughness profiles. To obtain the averaged roughness of the entire ROI of the dental crown inner surface, the sum of the left and right-side averaged roughness values was added to the averaged roughness of the bottom regions of the dental crown. To obtain normalized smoothness values, the averaged roughness of the inner surface of each dental crown specimen was calculated based on the pixel information. Next, the calculated each averaged roughness value was converted to smoothness value by using

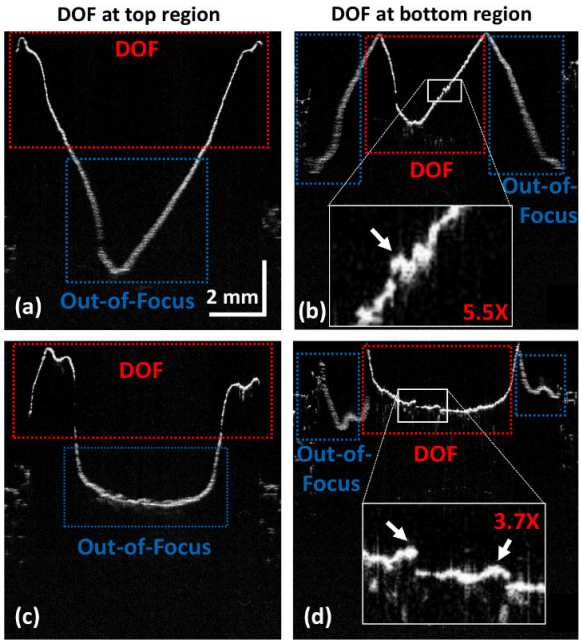

FIGURE 5. 2D cross-sectional images of a dental crown with the DOF set in two different regions. (a) The DOF was set at the topmost region of the dental crown. (b) The DOF was set at the bottom region of the crown. (c) The DOF at the topmost region of the crown when the scan position was shifted by 90° with respect to that used to record the image in (a). (d) The DOF at the bottom region of the crown when the scan position was shifted by 90° with respect to that used to record the image in (b).

the reciprocal of the averaged roughness values. Finally, all the smoothness values were normalized by dividing the obtained maximum smoothness values.

III. RESULTS AND DISCUSSION

A. QUANTITATIVE EVALUATION OF THE INNER SURFACE ROUGHNESS OF THE DENTAL CROWN

Figure 5 shows cross-sectional 2D OCT images of the inner surface of a 3D printed dental crown with the DOF matched to different regions of the sample. Figures 5(a and b) show the cross-sectional representations of the sagittal section planes and Figures 5(c and d) show the coronal section planes of the dental crown. For the data recorded and shown in Figures 5(a and c), the sample arm was placed at a distance in such a way that the DOF was matched to the topmost region of the dental crown, meaning that the bottom region of the sample appears out of focus. In contrast, for the data recorded and shown in Figures 5(b and d), the DOF was matched to the bottom region of the dental crown, meaning that the topmost region of the sample appears out of focus. The red-colored dotted rectangles in the images illustrate the regions where the DOF is precisely matched, while the blue colored dotted rectangles illustrate the regions where the DOF is only partially matched. Since intense peaks that indicate rough regions can be identified through the precise matching of the DOF, multiple DOFs were used during the measurements. It was observed that in the fully focused part of the dental crown (the red dashed boxes in Figures 5(b and d)) few visually observable peaks corresponding to the roughness can be identified (indicated by the white arrows). In the image processing algorithm, completely focused inner surface images such as those shown in Figures 5(a and b) were set as the ROI to calculate the inner surface roughness.

Figure 6 shows 2D cross-sectional images of dental crowns fabricated using three different hatching methods with build direction angles of 0°, 45°, and 90°, acquired using OCT imaging with the DOF set at the top and bottom regions of the dental crowns. Figures 6(a, b, c, g, h, i, m, n, and o) and (d, e, f, j, k, l, p, q, and r) were acquired with the DOF set at the topmost and bottom regions of the dental crowns, respectively. It can be seen from the images that the dental crown surfaces fabricated using build direction angles of 0° and 45° are rougher than those fabricated using a build direction angle of 90°. In the cross-sectional images, the highly rough areas of the surfaces of the dental crowns are indicated by red boxes. The most appropriate hatching method out of the three different methods used cannot be identified by simply looking at the 2D cross-sectional images because there is no significant difference in roughness between these images of the dental crowns.

A total number of nine 3D images were obtained of dental crowns fabricated using three different hatching methods, hatching methods 1, 2, and 3, and with three different build directions, are shown in Figures 7(a, b, and c), (d, e, and f), and (g, h, and i), respectively. Compared to hatching methods 1 and 3, the inner surface smoothness of the dental crowns printed using hatching method 2 (cross lamination at 0° and 90°, vertical and horizontal alternation) are high, and the samples show the most accurate stacking. In contrast, the dental crowns fabricated using hatching method 3 were found to be the roughest compared to those produced using the other hatching methods. Continuous rough regions (indicated by white dotted boxes) were identified in the surfaces of the crowns fabricated using both hatching methods 1 and 3, as shown in Figures 7(a, b, g, and h), whereas the surfaces of those produced using hatching method 2 have fewer rough areas that do not cover as much area as the continuous rough regions observed in the other hatching methods. Figures 7(a, d, and g), (b, e, and h), and (c, f, and i) show 3D images of the dental crowns fabricated with build direction angles of 0°, 45°, and 90°, respectively. Figures 7(c, f, and i) clearly show that the dental crowns printed in a build direction angle of 90° are much smoother than the other dental crowns fabricated in build direction angles of 0° and 45°. The dental crowns fabricated in build direction angles of 0° and 45° have continuous rough areas that cover a greater area, while at 90°, the surfaces of the crowns do not show extensively rough areas. As seen in Figure 7, the images of the surfaces of the samples printed with a build direction angle of 45° are comparatively rougher than those fabricated using 0° and 90° angles.

B. ANALYTICAL EVALUATION OF THE INNER SURFACE ROUGHNESS OF THE DENTAL CROWN

Normalized smoothness values of the inner surfaces of the dental crowns fabricated using hatching methods 1, 2, and 3

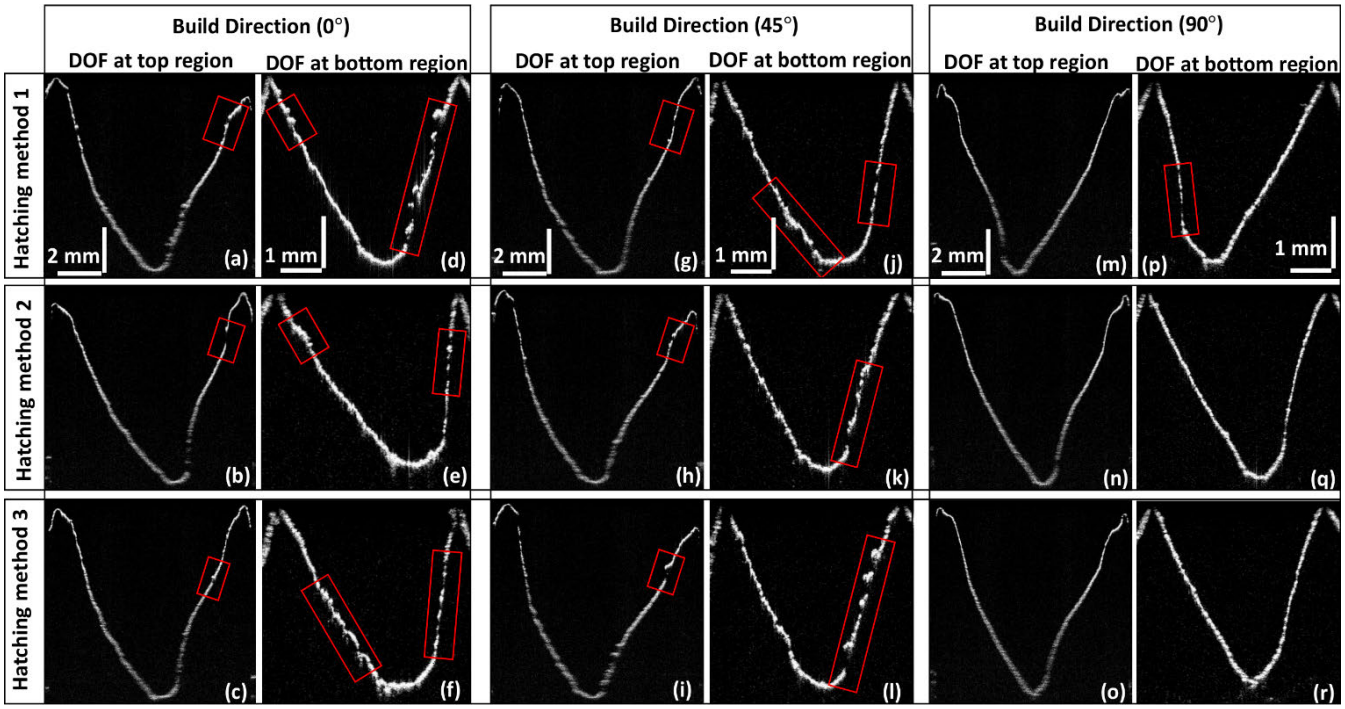

FIGURE 6. 2D cross-sectional images of dental crown samples fabricated using three different hatching methods with the DOF set at two different regions of the dental crowns. Images (a, d, g, j, m, and p), (b, e, h, k, n, and q), and (c, f, i, l, o, and r) show the dental crowns fabricated using hatching methods 1, 2, and 3, respectively. Images (a, b, c, g, h, i, m, n, and o) and (d, e, f, j, k, l, p, q, and r) show the DOF set at the topmost and bottom regions of the dental crowns, respectively.

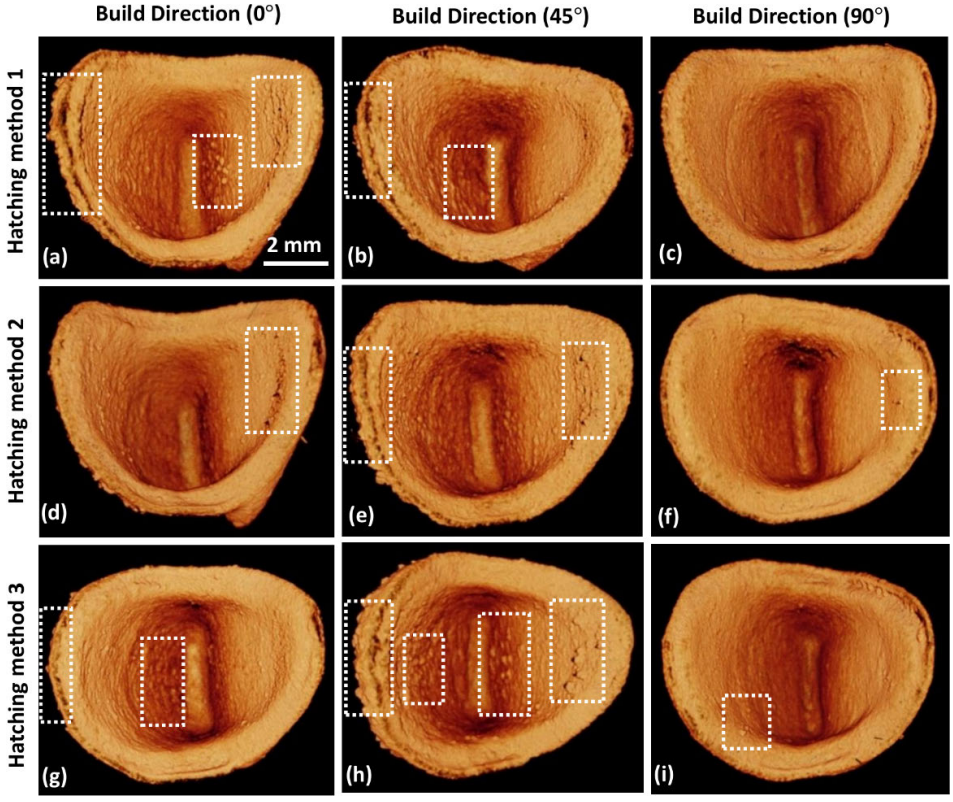

FIGURE 7. 3D images of the dental crowns fabricated using (a, b, and c) hatching method 1 (at build direction angles of 0°, 45°, and 90°, respectively), (d, e, and f) hatching method 2 (at build direction angles of 0°, 45°, and 90°, respectively), and (g, h and i) hatching method 3 (at build direction angles of 0°, 45°, and 90°, respectively).

in three different build directions are shown in Figures 8 (a, b, and c), respectively. It can be seen that for all of the hatching methods, the smoothness values of the samples prepared in a build direction of 90° angle are higher

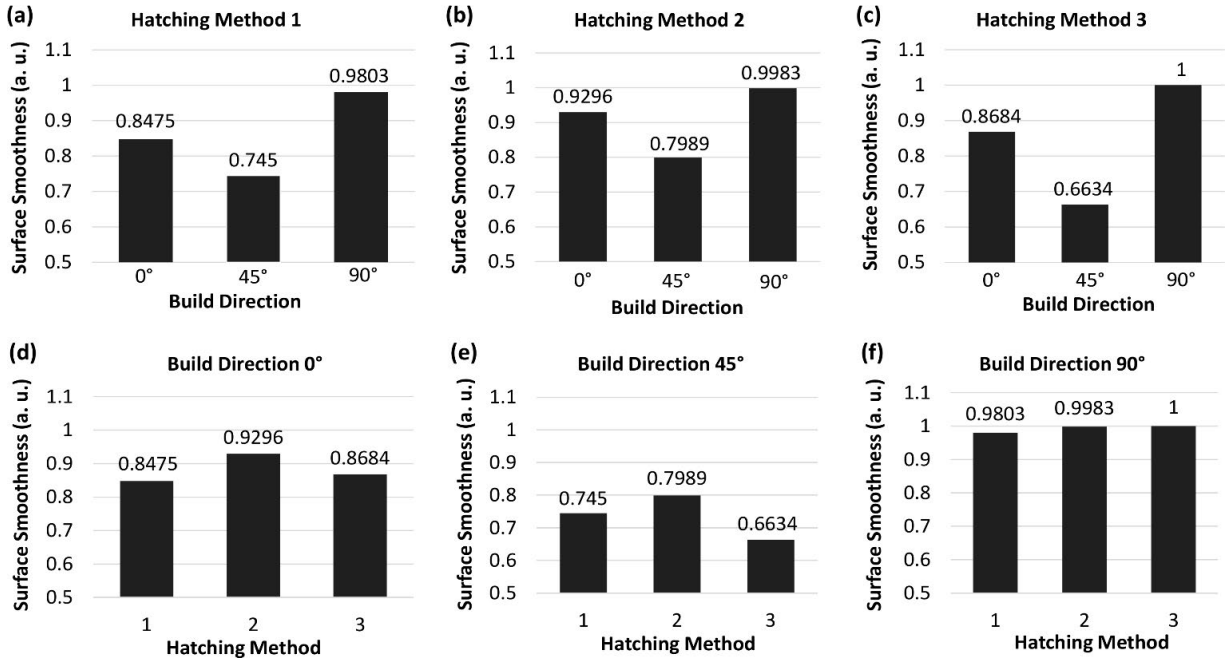

FIGURE 8. Graphs showing the normalized surface smoothness values of dental crowns fabricated using (a, b, and c) hatching methods 1, 2, and 3, respectively, and (d, e, and f) in build direction angles of 0°, 45°, and 90°, respectively.

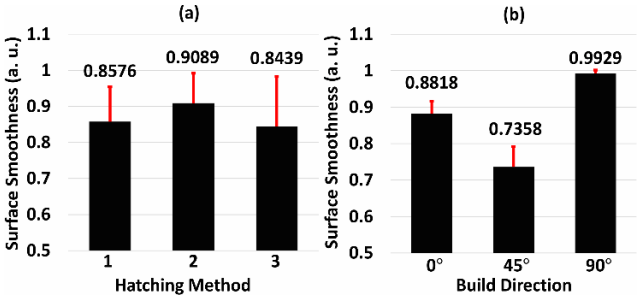

FIGURE 9. Inner surface averaged smoothness results of dental crowns printed using (a) three different hatching methods and (b) in three different build directions.

than those recorded for the 0° and 45° angles. It can also be seen that out of all the samples, the smoothness values of the samples prepared using the three hatching methods each with build direction angles of 45° angle are lower than those recorded for the samples made using the other build direction angles. Figures 8(d, e, and f) show the inner surface smoothness values of the dental crowns constructed in build direction angles of 0°, 45°, and 90°, respectively. In Figures 8(d and e), it can be seen that the inner surface smoothness values of hatching method 2 are higher than those of the other hatching methods. While in Figure 8(f), it can be observed that for a build direction angle of 90°, the surface smoothness values of hatching methods 2 and 3 are almost the same and higher than those of hatching method 1.

Figure 9(a) shows the calculated normalized and averaged (averages of the build direction angles of 0°, 45°, and 90°) smoothness results of the dental crown samples fabricated using three different hatching methods. From Figure 9(a), it can be seen that the averaged surface smoothness of the dental crowns printed using hatching method 2 is greater than for the other hatching methods, in three different build directions. Figure 9(b) shows the normalized and averaged (average of the three hatching methods) smoothness results of the dental crowns printed in build direction angles of 0°, 45°, and 90°. From the same figure, it can be seen that the averaged surface smoothness of the dental crowns printed in build direction angles of 90° using the three different hatching methods is greater than that of the samples printed at 0° and 45° angles.

Cross-hatching (hatching method 2) was found to be the most useful of the three hatching methods used, with a normalized and averaged smoothness value of 0.9089, greater than those of the dental crowns printed using the other methods. The standard deviations of hatching methods 1, 2, and 3 in the three different build directions are 0.0963, 0.0827, and 0.1385, respectively. The build direction also seems to have a direct impact on the surface smoothness of the fabricated dental crowns. In particular, when the build direction is below 45°, it directly contributes toward the increased roughness of the surface of the fabricated dental crown and harms the inner surface of the final product, which may affect the bonding effectiveness of the crown. The build direction angle of 90° was found to produce samples with the best inner surface smoothness of 0.9929±0.0089 (mean±standard deviation), whereas the samples prepared using the build direction angle of 45° showed the worst surface smoothness value of 0.7358 ± 0.0557. The variance (0.0280) of the hatching methods was determined to be 3.76 times more stable than the variance (0.1053) of the build directions in terms of the inner surface stability of samples produced using 3D printing. The combination of hatching method 3 and 90°

angle build direction fabricated a dental crown sample with the highest smoothness value, was determined by using the roughness quantification algorithm. Furthermore, the triple imaging attempts of the inner surface with DOF at the top, middle, and bottom regions of the dental crown, was also considered due to the deep height of the samples. However, most regions of the inner surface of the dental crown were sufficiently measured. A small gap of the uncovered region in two times imaging (DOF at top and bottom regions of the dental crown) did not change the main consequence to the aim of the assessment and comparison of the hatching methods and building directions in this experiment. OCT has potential merits in the current study since a ground truth imaging modality for the assessment of inner surface roughness has not been descriptively presented to date due to challenging technical limitations of measuring whole inner surface roughness of dental crown. Although OCT is difficult to be determined as the gold standard without a precise comparison with any ground truth imaging modality applied in the inner surface evaluation, the feasibility of OCT system and the customized image processing algorithm was sufficiently verified in this research.

IV. CONCLUSION

An SS-OCT system was used to identify the optimal way of fabricating dental prostheses via a commercial 3D printing SLM method. In the 3D fabrication of dental prostheses, three different build directions angles (0°, 45°, and 90°) and three different hatching methods (one-way, cross, and 30° counter-clockwise) were used and the roughness values of the inner surface of the samples were measured using a developed roughness measurement algorithm. As the cooling of printed layers is a part of the fabrication process, subsequently this affects the smoothness of the dental crowns. If during the fabrication process the stacking of layers is in the same direction, i.e., repeated in one direction only, this may result in a variation in thickness during the cooling process, affecting the precision of the 3D printed sample layers. This can be avoided by controlling the cooling process, which can be achieved by hatching in the cross lamination method. Also, stepwise stacking minimizes the chances of any abrupt changes occurring in the shape of the printed dental crowns. The aim of this study was to confirm the potential applicability of SS-OCT based roughness assessment algorithm to determine the most appropriate hatching method and build direction in 3D fabrication by assessing the inner surface roughness of the 3D printed dental crowns during fabrication, which has significant merits over existing methods. The usefulness of the SS-OCT system was successfully demonstrated for 3D printed fabrications with high-resolution, cross-sectional, and real-time imaging in 3D dental printing fields, where the assessment was challenging using conventional methods. Since the proposed method was performed to confirm how feasible is OCT to obtain the desired result and confirm hatching methods and build direction, statistical results were not included with a large number of samples. However, the acquired results successfully revealed the implementation of OCT imaging for determining the most appropriate hatching method and build direction in 3D fabrication by assessing the inner surface roughness of dental crown using the developed image processing algorithm based on OCT cross-sectional images, where it is challenging for the conventional imaging and roughness assessment methods due to technical limitations of imaging and measuring whole inner surface roughness of dental crown. In conclusion, the verified results of the proposed study can be more utilized to evaluate the quality assurance of the 3D printed fabrication in dental fields.

ACKNOWLEDGMENT

The authors would like to express their deepest thanks to researchers from the Laser Application Center, Institute of Advanced Convergence Technology for their support and assistance in this study. The authors also wish to acknowledge the contributions of Naresh Kumar Ravichandran, Deokmin Jeon, Kanghae Kim, Sangyeob Han, and Pilun Kim. *(Jaeyul Lee and Sm Abu Saleah contributed equally to this work.)*

REFERENCES

[1] F. Isidor, K. Brøndum, H. J. Hansen, J. Jensen, and S. Sindet-Pedersen, "Outcome of treatment with implant-retained dental prostheses in patients with Sjögren syndrome," *Int. J. Oral Maxillofacial Implants*, vol. 14, no. 5, pp. 736–743, 1999.

[2] G. A. Zarb and A. Schmitt, "The longitudinal clinical effectiveness of osseointegrated dental implants: The toronto study. Part II: The prosthetic results," *J. Prosthetic Dentistry*, vol. 64, no. 1, pp. 53–61, Jul. 1990.

[3] M. T. Kattadiyil, Z. Mursic, H. AlRumaih, and C. J. Goodacre, "Intraoral scanning of hard and soft tissues for partial removable dental prosthesis fabrication," *J. Prosthetic Dentistry*, vol. 112, no. 3, pp. 444–448, Sep. 2014.

[4] F. Beuer, H. Aggstaller, D. Edelhoff, W. Gernet, and J. Sorensen, "Marginal and internal fits of fixed dental prostheses zirconia retainers," *Dental Mater.*, vol. 25, no. 1, pp. 94–102, Jan. 2009.

[5] L. Zuskova, N. A. A. Mortadi, R. J. Williams, K. H. Alzoubi, and O. F. Khabour, "Comparison of overall fit of milled and laser-sintered CAD/CAM crown copings," *Int. J. Dentistry*, vol. 2019, pp. 1–5, Jul. 2019.

[6] K.-B. Kim, W.-C. Kim, H.-Y. Kim, and J.-H. Kim, "An evaluation of marginal fit of three-unit fixed dental prostheses fabricated by direct metal laser sintering system," *Dental Mater.*, vol. 29, no. 7, pp. e91–e96, Jul. 2013.

[7] A. Örtorp, D. Jönsson, A. Mouhsen, and P. Vult von Steyern, "The fit of cobalt–chromium three-unit fixed dental prostheses fabricated with four different techniques: A comparative in vitro study," *Dental Mater.*, vol. 27, no. 4, pp. 356–363, Apr. 2011.

[8] Y. S. Al Jabbari, T. Koutsoukis, X. Barmpagadaki, and S. Zinelis, "Metallurgical and interfacial characterization of PFM Co–Cr dental alloys fabricated via casting, milling or selective laser melting," *Dental Mater.*, vol. 30, no. 4, pp. e79–e88, Apr. 2014.

[9] N. Alharbi, R. Osman, and D. Wismeijer, "Factors influencing the dimensional accuracy of 3D-printed full-coverage dental restorations using stereolithography technology," *Int. J. Prosthodontics*, vol. 29, no. 5, pp. 503–510, Sep. 2016.

[10] R. Osman, N. Alharbi, and D. Wismeijer, "Build angle: Does it influence the accuracy of 3D-printed dental restorations using digital light-processing technology?" *Int. J. Prosthodontics*, vol. 30, no. 2, pp. 182–188, Mar. 2017.

[11] A. J. Zissis, G. L. Polyzois, S. A. Yannikakis, and A. Harrison, "Roughness of denture materials: A comparative study," *Int. J. Prosthodontics*, vol. 13, no. 2, pp. 136–140, 2000.

[12] M. Quirynen and C. Bollen, "The influence of surface roughness and surface-free energy on supra-and subgingival plaque formation in man: A review of the literature," *J. Clin. Periodontol.*, vol. 22, no. 1, pp. 1–14, 1995.

[13] J. S. Rahal, M. F. Mesquita, G. E. P. Henriques, and M. A. A. Nobilo, "Surface roughness of acrylic resins submitted to mechanical and chemical polishing," *J. Oral Rehabil.*, vol. 31, no. 11, pp. 1075–1079, Nov. 2004.

[14] C. M. L. Bollenl, P. Lambrechts, and M. Quirynen, "Comparison of surface roughness of oral hard materials to the threshold surface roughness for bacterial plaque retention: A review of the literature," *Dental Mater.*, vol. 13, no. 4, pp. 258–269, Jul. 1997.

[15] S. Hegde, P. Madhyastha, N. Srikant, R. Kotian, and S. Iyer, "Effect of finishing/polishing techniques and time on surface roughness of esthetic restorative materials," *Dental Res. J.*, vol. 14, no. 5, p. 326, 2017.

[16] M. Zortuk, K. Kilic, G. Uzun, A. Ozturk, and B. Kesim, "The effect of different fiber concentrations on the surface roughness of provisional crown and fixed partial denture resin," *Eur. J. Dentistry*, vol. 02, no. 03, pp. 185–190, Jul. 2008.

[17] U. En, "Advanced technical ceramics–monolithic ceramics–general and textural properties—Part 4: determination of surface roughness," Tech. Rep., 2005.

[18] W. M. Al-Omari, C. A. Mitchell, and J. L. Cunningham, "Surface roughness and wettability of enamel and dentine surfaces prepared with different dental burs," *J. Oral Rehabil.*, vol. 28, no. 7, pp. 645–650, Jul. 2001.

[19] A. Kakaboura, M. Fragouli, C. Rahiotis, and N. Silikas, "Evaluation of surface characteristics of dental composites using profilometry, scanning electron, atomic force microscopy and gloss-meter," *J. Mater. Sci., Mater. Med.*, vol. 18, no. 1, pp. 155–163, Jan. 2007.

[20] S. Kasas and A. Ikai, "A method for anchoring round shaped cells for atomic force microscope imaging," *Biophys. J.*, vol. 68, no. 5, pp. 1678–1680, May 1995.

[21] C. Sandobal, E. Carbó, J. Iribas, S. Roverano, and S. Paira, "Ultrasound nail imaging on patients with psoriasis and psoriatic arthritis compared with rheumatoid arthritis and control subjects," *J. Clin. Rheumatol.*, vol. 20, no. 1, pp. 21–24, Jan. 2014.

[22] E. Sattler, R. Kaestle, G. Rothmund, and J. Welzel, "Confocal laser scanning microscopy, optical coherence tomography and transonychial water loss for *in vivo* investigation of nails," *Brit. J. Dermatol.*, vol. 166, no. 4, pp. 740–746, Apr. 2012.

[23] A. C. S, P. Damberg, S. N. Aski, K. Nagy, C. E. Berglin, and G. Laurell, "Experimental fusion of contrast enhanced high-field magnetic resonance imaging and high-resolution micro-computed tomography in imaging the mouse inner ear," *Open Neuroimag. J.*, vol. 9, no. 1, pp. 7–12, Jul. 2015.

[24] D. J. Brenner and E. J. Hall, "Computed tomography-an increasing source of radiation exposure," *New England J. Med.*, vol. 357, no. 22, pp. 2277–2284, 2007.

[25] D. L. Price, J. P. De Wilde, A. M. Papadaki, J. S. Curran, and R. I. Kitney, "Investigation of acoustic noise on 15 MRI scanners from 0.2 t to 3 t," *J. Magn. Reson. Imag.*, vol. 13, no. 2, pp. 288–293, 2001.

[26] J. G. Fujimoto, C. Pitris, S. A. Boppart, and M. E. Brezinski, *Optical Coherence Tomography: An Emerging Technology for Biomedical Imaging and Optical Biopsy*, vol. 2. New York, NY, USA: Neoplasia, 2000, p. 9.

[27] J. Lee, M. F. Shirazi, K. Park, M. Jeon, and J. Kim, "Defect inspection of actuator lenses using swept-source optical coherence tomography," *Opt. Rev.*, vol. 25, no. 3, pp. 403–409, Jun. 2018.

[28] S. Kishi, "Impact of swept source optical coherence tomography on ophthalmology," *Taiwan J. Ophthalmol.*, vol. 6, no. 2, pp. 58–68, Jun. 2016.

[29] M. Adhi and J. S. Duker, "Optical coherence tomography–current and future applications," *Current Opinion Ophthalmol.*, vol. 24, no. 3, p. 213, 2013.

[30] M. Rubinstein, P. Schalch, M. Di Silvio, M. A. Betancourt, and B. J. Wong, "Optical coherence tomography applications in otolaryngology," *Acta Otorrinolaringol. (English Ed.)*, vol. 60, no. 5, pp. 357–363, 2009.

[31] J. A. Izatt, M. D. Kulkarni, H.-W. Wang, K. Kobayashi, and M. V. Sivak, "Optical coherence tomography and microscopy in gastrointestinal tissues," *IEEE J. Sel. Topics Quantum Electron.*, vol. 2, no. 4, pp. 1017–1028, Dec. 1996.

[32] D. Choi, J. Lee, M. Jeon, and J. Kim, "*In vivo* fascicle bifurcation imaging of rat sciatic nerve using swept-source optical coherence tomography," *IEEE Access*, vol. 6, pp. 7713–7718, 2018.

[33] J. Lee, K. Kim, R. E. Wijesinghe, D. Jeon, S. H. Lee, M. Jeon, and J. H. Jang, "Decalcification using ethylenediaminetetraacetic acid for clear microstructure imaging of cochlea through optical coherence tomography," *J. Biomed. Opt.*, vol. 21, no. 8, Mar. 2016, Art. no. 081204.

[34] J. Lee, R. E. Wijesinghe, D. Jeon, P. Kim, Y.-H. Choung, J. H. Jang, M. Jeon, and J. Kim, "Clinical utility of intraoperative tympanomastoidectomy assessment using a surgical microscope integrated with an optical coherence tomography," *Sci. Rep.*, vol. 8, no. 1, p. 17432, Dec. 2018.

[35] K. Brown and M. Harvey, "Optical coherence tomography: Age estimation of Calliphora vicina pupae *in vivo*?" *Forensic Sci. Int.*, vol. 242, pp. 157–161, Sep. 2014.

[36] N. Ravichandran, R. Wijesinghe, S.-Y. Lee, K. Choi, M. Jeon, H.-Y. Jung, and J. Kim, "Non-destructive analysis of the internal anatomical structures of mosquito specimens using optical coherence tomography," *Sensors*, vol. 17, no. 8, p. 1897, Aug. 2017.

[37] K. Kim, P. Kim, J. Lee, S. Kim, S. Park, S. H. Choi, J. Hwang, J. H. Lee, H. Lee, R. E. Wijesinghe, M. Jeon, and J. Kim, "Non-destructive identification of weld-boundary and porosity formation during laser transmission welding by using optical coherence tomography," *IEEE Access*, vol. 6, pp. 76768–76775, 2018.

[38] F. A. M. Saccon, M. Muller, and J. L. Fabris, "Optical fiber characterization by optical coherence tomography," in *IEEE MTT-S Int. Microw. Symp. Dig.*, Nov. 2009, pp. 625–628.

[39] R. E. Wijesinghe, K. Park, Y. Jung, P. Kim, M. Jeon, and J. Kim, "Industrial resin inspection for display production using automated fluid-inspection based on multimodal optical detection techniques," *Opt. Lasers Eng.*, vol. 96, pp. 75–82, Sep. 2017.

[40] N. K. Ravichandran, R. E. Wijesinghe, M. F. Shirazi, K. Park, M. Jeon, W. Jung, and J. Kim, "Depth enhancement in spectral domain optical coherence tomography using bidirectional imaging modality with a single spectrometer," *J. Biomed. Opt.*, vol. 21, no. 7, Jul. 2016, Art. no. 076005.

[41] T. Anna, S. Chakraborty, C.-Y. Cheng, V. Srivastava, A. Chiou, and W.-C. Kuo, "Elucidation of microstructural changes in leaves during senescence using spectral domain optical coherence tomography," *Sci. Rep.*, vol. 9, no. 1, p. 1167, Dec. 2019.

[42] Y. S. Hsieh, Y. C. Ho, S. Y. Lee, C. C. Chuang, J. Tsai, and K. F. Lin, "Dental optical coherence tomography," *Sensors*, vol. 13, no. 7, pp. 8928–8949, Jul. 2013, doi: 10.3390/s130708928.

[43] A. Baumgartner, S. Dichtl, and C. K. Hitzenberger, "Polarization–sensitive optical coherence tomography of dental structures," *Caries Res.*, vol. 34, no. 1, pp. 59–69, 2000.

[44] R. Wijesinghe, N. Cho, K. Park, M. Jeon, and J. Kim, "Bio-photonic detection and quantitative evaluation method for the progression of dental caries using optical frequency-domain imaging method," *Sensors*, vol. 16, no. 12, p. 2076, Dec. 2016.

[45] S. Lee, K. Son, J. Park, J. Lee, S. H. Kang, R. E. Wijesinghe, P. Kim, J. H. Hwang, S. Park, B.-J. Yun, M. Jeon, K.-B. Lee, and J. Kim, "Non-ionized, high-resolution measurement of internal and marginal discrepancies of dental prosthesis using optical coherence tomography," *IEEE Access*, vol. 7, pp. 6209–6218, 2019.

[46] J. Lee, J. Park, M. Faizan Shirazi, H. Jo, P. Kim, R. E. Wijesinghe, M. Jeon, and J. Kim, "Classification of human gingival sulcus using swept-source optical coherence tomography: *in vivo* imaging," *Infr. Phys. Technol.*, vol. 98, pp. 155–160, May 2019.

[47] N. K. Ravichandran, H. Cho, J. Lee, S. Han, R. E. Wijesinghe, P. Kim, J.-W. Song, M. Jeon, and J. Kim, "An averaged intensity difference detection algorithm for identification of human gingival sulcus in optical coherence tomography images," *IEEE Access*, vol. 7, pp. 73076–73084, 2019.

[48] N. K. Ravichandran, H. Tumkur Lakshmikantha, H.-S. Park, M. Jeon, and J. Kim, "Analysis of enamel loss by prophylaxis and etching treatment in human tooth using optical coherence tomography: An in vitro study," *J. Healthcare Eng.*, vol. 2019, pp. 1–9, Mar. 2019.

[49] H. T. Lakshmikantha, N. K. Ravichandran, M. Jeon, J. Kim, and H.-S. Park, "3-Dimensional characterization of cortical bone microdamage following placement of orthodontic microimplants using Optical Coherence Tomography," *Sci. Rep.*, vol. 9, no. 1, p. 3242, Dec. 2019.

[50] A. Tahayeri, M. Morgan, A. P. Fugolin, D. Bompolaki, A. Athirasala, C. S. Pfeifer, J. L. Ferracane, and L. E. Bertassoni, "3D printed versus conventionally cured provisional crown and bridge dental materials," *Dental Mater.*, vol. 34, no. 2, pp. 192–200, Feb. 2018.

JAEYUL LEE is currently pursuing the Ph.D. degree with the School of Electronics Engineering, Kyungpook National University, Daegu, South Korea. His research interests include the development of high-resolution novel imaging techniques and optical imaging techniques, including photoacoustic microscopy, optical coherence tomography, optical coherence angiography, handheld instruments, and their biomedical applications.

SM ABU SALEAH received the B.Sc. degree in telecommunication and electronic engineering from Hajee Mohammad Danesh Science and Technology University, Dinajpur, Bangladesh, and the M.Sc. degree in information technology from the Institute of Information Technology, Jahangirnagar University, Dhaka, Bangladesh. He has been a Ph.D. Researcher with the Electronics Engineering Department, Kyungpook National University, since 2019. His research interests include the development of novel biological and biomedical imaging techniques, including optical coherence tomography, photoacoustic tomography and microscopy, and their clinical applications.

BYEONGGYU JEON received the B.E. degree in electronics engineering from Kyungpook National University, Daegu, South Korea, in 2018, where he is currently pursuing the M.S. degree with the Electronics Engineering Department. His research interests include the development of biomedical imaging systems, including optical coherence tomography, photoacoustic tomography, and their clinical applications.

RUCHIRE ERANGA WIJESINGHE received the B.Sc. and Ph.D. degrees in electronics engineering from Kyungpook National University, Daegu, South Korea, in 2012 and 2018, respectively. He is currently an Assistant Professor at the Department of Biomedical Engineering, Kyungil University. His research interests include the development of high-resolution novel biological and biomedical imaging techniques, including optical coherence tomography and microscopy for clinical utility.

DONG-EUN LEE worked as an Assistant Professor with the School of Engineering, Southern Illinois University Edwardsville (SIUE), USA. He is currently a Full Professor with tenure at the School of Architecture and Civil Engineering and at the Robot and Smart System Engineering, Kyungpook National University, South Korea. He is also the Chief of the Intelligent Construction Automation Center nominated by the Ministry of Science and ICT. His research interests include automation in construction, construction robot, optimization, stochastic simulation, and quantitative analysis.

MANSIK JEON (Member, IEEE) received the Ph.D. degree in electronics engineering from Kyungpook National University, Daegu, South Korea, in 2011. He is currently an Associate Professor at the School of Electronics Engineering, Kyungpook National University. His research interests include the development of nonionizing and noninvasive novel biomedical imaging techniques, including photoacoustic tomography, photoacoustic microscopy, optical coherence tomography, ultrasonic imaging, handheld scanner, and their clinical applications.

JEEHYUN KIM (Member, IEEE) received the Ph.D. degree in biomedical engineering from The University of Texas at Austin, USA, in 2004. He worked as a Postdoctoral Researcher at the Beckman Laser Institute, University of California at Irvine. He is currently a Professor at Kyungpook National University, Daegu, South Korea. His research interests include biomedical imaging and sensing, neuroscience studies using multiphoton microscopy, photo-acoustic imaging, and other novel applications of sensors.